Science of the Total Environment 572 (2016) 1–8

Contents lists available at ScienceDirect

Science of the Total Environment

journal homepage: www.elsevier.com/locate/scitotenv

Atmospheric thorium pollution and inhalation exposure in the largest rare earth mining and smelting area in China

Lingqing Wang [a,*], Buqing Zhong [a], Tao Liang [a], Baoshan Xing [b], Yifang Zhu [c,*]

[a] Key Laboratory of Land Surface Pattern and Simulation, Institute of Geographical Sciences and Natural Resources Research, Chinese Academy of Sciences, Beijing 100101, China
[b] Stockbridge School of Agriculture, University of Massachusetts, Amherst, MA 01003, USA
[c] Department of Environmental Health Sciences, Jonathan and Karin Fielding School of Public Health, University of California, Los Angeles, CA 90095, USA

HIGHLIGHTS

- Atmospheric thorium pollution was investigated around the Bayan Obo rare earth mine.
- ^{232}Th concentrations were significantly higher than the world reference of 0.5 μBq m^{-3}.
- A self-organizing map was used to identify spatiotemporal pattern of airborne thorium.
- The inhalation exposure results show a high radioactive risk for local dwellers.

GRAPHICAL ABSTRACT

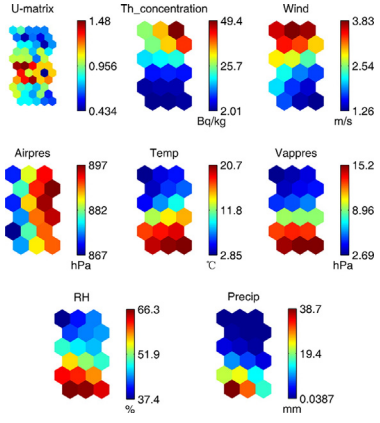

ARTICLE INFO

Article history:
Received 15 May 2016
Received in revised form 26 July 2016
Accepted 27 July 2016
Available online xxxx

Editor: D. Barcelo

Keywords:
Thorium
Rare earth
TSP
PM_{10}
Inhalation exposure

ABSTRACT

Exposure to radionuclide thorium (Th) has generated widespread public concerns, mainly because of its radiological effects on human health. Activity levels of airborne ^{232}Th in total suspended particulate (TSP) were measured in the vicinity of the largest rare earth mine in China in August 2012 and March 2013. The mean activity concentrations of ^{232}Th in TSP ranged from 820 μBq m^{-3} in a mining area in August 2012 to 39,720 μBq m^{-3} in a smelting area in March 2013, much higher than the world reference of 0.5 μBq m^{-3}. Multistatistical analysis and Kohonen's self-organizing maps suggested that ^{232}Th in TSP was mainly derived from rare earth mining and smelting practices. In addition, personal inhalation exposures to ^{232}Th associated with respirable particulate (PM_{10}) were also measured among local dwellers via personal monitoring. The mean dose values for different age groups in the smelting and mining areas ranged from 97.86 to 417 μSv year^{-1} and from 101.03 to 430.83 μSv year^{-1}, respectively. These results indicate that people living in the study areas are exposed to high levels of widespread ^{232}Th.

© 2016 Elsevier B.V. All rights reserved.

1. Introduction

Thorium (Th) is a primordial radioactive element which is ubiquitous in the environment at varying concentrations. >99% of natural thorium exist in the form of ^{232}Th, which has a long half-life

* Corresponding authors.
E-mail addresses: wanglq@igsnrr.ac.cn (L. Wang), yifang@ucla.edu (Y. Zhu).

http://dx.doi.org/10.1016/j.scitotenv.2016.07.192
0048-9697/© 2016 Elsevier B.V. All rights reserved.

(1.39×10^{10} year) and low specific activity (4.1 kBq g^{-1}) (Höllriegl et al., 2007). Numerous investigations over the past decade have focused on the ^{232}Th concentration in rocks, soils, water bodies and sediments and the potential external radiation dose to the public (Cowart and Burnett, 1994; Kritsananuwat et al., 2015). However, research on airborne ^{232}Th activity concentrations is still limited because of analytical limitations.

Thorium can be released into the atmosphere from both natural and anthropogenic sources that elevate its level over the background, including substances in Earth's crust, cosmic rays, volcano eruption, nuclear fuel plants, coal combustion, and ore mining and refining (Cowart and Burnett, 1994; Alvarado et al., 2014). Atmospheric particulate matter (PM) contaminated with ^{232}Th are harmful to human health due to increased radiotoxicity and chemotoxicity. Studies revealed that ^{232}Th if inhaled as a dust or accumulated in human body increased the risk of lung and liver diseases, lung and pancreatic cancer, adverse effect on blood and changes in human genetic material (Soudek et al., 2013). It is estimated that more than half of total radioactive dose received by world's population is associated with inhalation of radioactive aerosol particles (United Nations Scientific Committee on Effects of Atomic Radiation, UNSCEAR, 2000). Therefore, it is of importance to investigate the activity level of Thorium in aerosols, particularly the respirable PM (PM_{10}), which contributes significantly to internal radiation dose and may subsequently cause adverse health effects.

Nearly all rare earth ores contain the radioactive elements thorium and uranium (Binnemans and Jones, 2015). The Bayan Obo deposit in North China contains the largest rare earth resources in the world. Its rare earth mineral is concomitant with natural radiothorium in the ThO_2 with a mean concentration of 0.04% by weight (Chen et al., 2005). Since the discovery of the main ore body in 1927, mining activities had been carried out over 90 years. Intensive exploitation activities of rare earth resources have caused the substantial increases of ^{232}Th contents in the environment (Li et al., 2014). Thorium was released into the atmosphere as aerosol particles from mining, milling, processing operations of rare earth minerals, and particle resuspension from tailing piles. Residents living around the mining and smelting areas are likely exposed to the radioactive aerosols with ^{232}Th through inhalation, ingestion of food and water contaminated by the fallout of particles, and dermal contact with fallout.

Kohonen's self-organizing maps (SOM), which is based on an unsupervised neural network model, can serve as an important tool for pattern recognition and classification without preliminary knowledge of the process (Mukherjee, 1997; García and González, 2004). SOM potentially outperforms other multivariate techniques such as principle component analysis for its visualizing interpretation, powerful clustering capability, and ability to deal with nonlinear problems (Hong et al., 2003; Aguado et al., 2008). SOM has been frequently used for pollutants pattern recognition in various environmental media (Lee and Scholz, 2006; Nadal et al., 2006; Gulson et al., 2007; Mari et al., 2010). In the present study, aerosol samples of total suspended particulate (TSP) and PM_{10} were collected from two sampling sites in the largest rare earth industry city, one in the Bayan Obo rare earth mining area and the other in the nearby smelting areas. We used the SOM model to identify the most impacted zones and to assess the potential correlations between thorium in aerosols and meteorological factors. Such research will provide a basis for understanding the impact of thorium emissions on the atmospheric environment and human health due to the rare earth smelting and mining activities.

2. Materials and methods

2.1. Study area

Baotou city (Fig. 1, 40°14′56″–42°43′49″N, 109°15′12″–111°26′25″E) is the largest rare earth industrial base and accounts for >70% of total rare earth production in China (Zhu et al., 2015). This region has a typical arid continental climate, characterized by windy and dry winter and spring, and warm and comparatively wet summer followed by short and cool autumn (Li et al., 2002). Mean annual temperature is around 6.5 °C, and the lowest and highest monthly mean temperatures are −11.1 °C in January and 23.3 °C in July, respectively. The average annual precipitation is about 240–400 mm, of which over 67% falls in the summer months (June–August). Mean annual evaporation is around 1938–2342 mm, several times greater than the annual precipitation. Prevailing wind directions are northwest in winter and spring, and southwest to south in summer and autumn. On a 50-year average, the annual wind speed is 3.1 m s^{-1} and the number of days with strong wind (≥17 m s^{-1}), floating dust, and the dust storm are about 46, 26 and 43 per year, respectively. After the cold and dry winter, aeolian sand activity is strong and frequent in spring (March to May) because of high air pressure gradients between the Siberian mainland and East Asia.

The giant Bayan Obo Fe–RE–Nb deposit comprises >170 different minerals. Its total reserves have been reported as at least 1.5 billion tonnes of iron (average grade 35%), 48 million tonnes of rare earth oxides (average grade 6%), and about 1 million tonnes of niobium (average grade 0.13%) (Wu, 2008). The concentrates after ore beneficiation used for rare earth production usually contain about 50–60% REO and 0.18–0.3% ThO_2 (Zhu et al., 2015). It is estimated that refining one tonne of rare earth oxide can potentially produce 6×10^4 m^3 of waste gas, 200 m^3 of acidic water and 1.4 tonnes of radioactive waste (Hao et al., 2015). Reports indicate that 96%–98% of Bayan Obo's thorium ends up in solid waste, 0.1%–0.5% is emitted as exhaust gas, and 0.6%–2.0% goes to liquid effluents (Ault et al., 2015). Long-term mining activities have produced a large amount of tailings which discharged into the reservoir through open slots by circulating water. The openly dumped tailing covers an area of 11.5 km^2 with thorium-radioactive tailings of 1.5×10^8 tonnes. After water is evaporated from the tailing pond, part of the tailing area is exposed to the air. The tailing powder was easily spread to the surrounding environment with strong wind. This process will inevitably result in elevated levels of ^{232}Th in the surrounding areas and cause adverse effects on human health (Chen et al., 2004). Therefore, it is necessary to characterize and quantify the natural radioactive content in TSP and PM_{10} to evaluate the associated environmental and human health risks.

2.2. Sampling and measurement

TSP samples were collected from 5 sites (Y01–Y05) in the rare earth mining area and 13 sites (B01–B13) in the smelting area in Baotou (Fig. 1). The intelligent medium-volume air sampler (TH-150C, Wuhan Tianhong Instrument Co., Ltd., China) and 90-mm quartz microfiber filters were used to collect TSP samples. The sampling flow rate was fixed at 100 L min^{-1}. At each site, 12-h samples were collected for three days from 8:00 am to 8:00 pm in 14th–20th August 2012 and 16th–22th March 2013, respectively. The sampling periods were chosen to avoid rainy days and most of the sampling at different sites was performed concurrently. A total of 104 TSP samples were collected from three consecutive days at both sampling sites.

To evaluate the radiation risk of inhalation exposure, 10 volunteers from the Kuangshan community near the mining area and 9 volunteers from the Wulanji community around the smelting area were randomly selected to wear a personal inhalation exposure sampler with a 10-μm cut-size (Omni5000IS, Beijing Jinkesantong Instrument Co., Ltd., China) to collect PM_{10} samples. Each sampler (flow rate 3 L min^{-1}) was placed at the breathing zone of the volunteers for 24 h from 8:00 am to 8:00 am the next day. Three samples were obtained from each volunteer for three consecutive days. The PM_{10} samples were collected on 37-mm quartz microfiber filters.

Prior to use, the filters of both Φ90 mm and Φ37 mm (Pore size = 0.2 μm, retention >99%, MK360, Munktell, Sweden) were pre-baked in a muffle furnace at 450 °C for at least 4 h and then maintained in a refrigerator (2 °C) for over 24 h and weighed before and after sampling. The mass

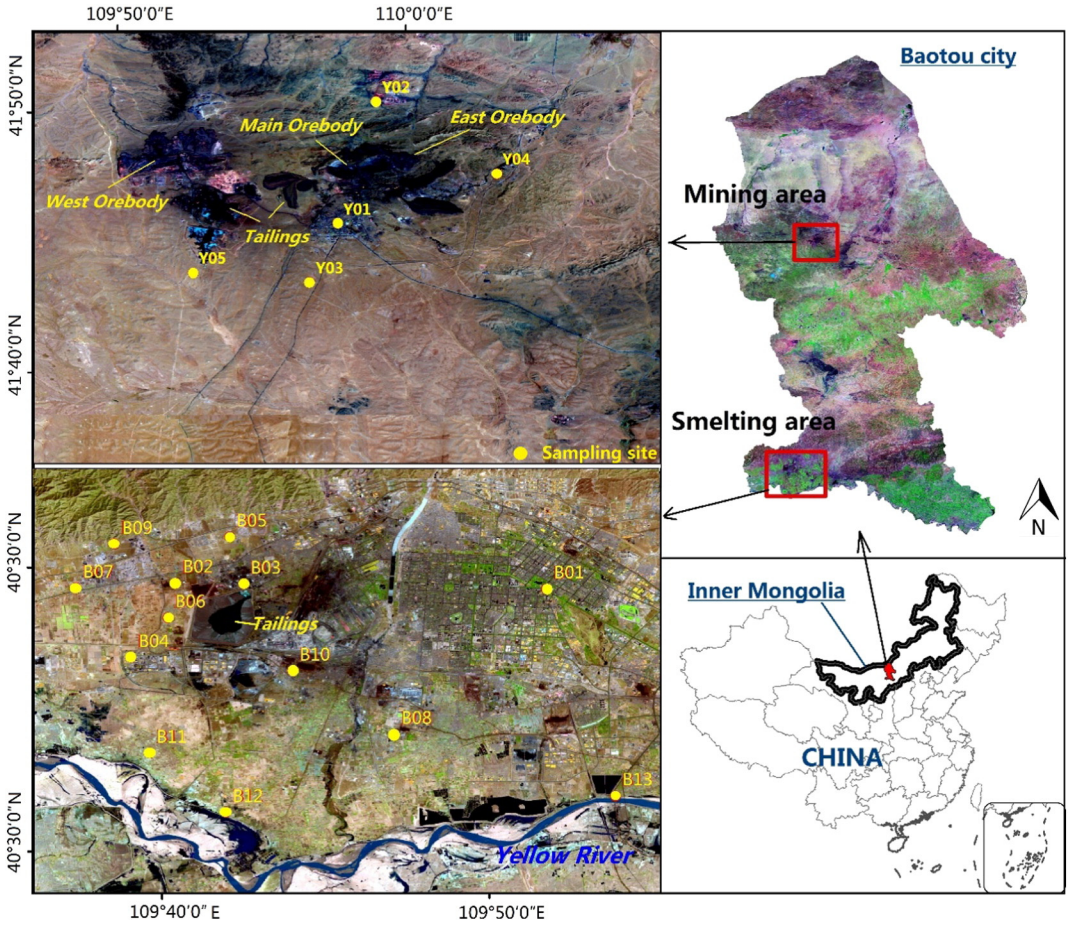

Fig. 1. Study area and sampling sites.

difference of the filters before and after sampling and the amount of sampled air volume were used for the TSP and PM_{10} concentration calculations.

The sampled filters were cut into small pieces using plastic scissors and subsequently stored in an air-tight cylindrical Teflon container, mixed with 5 mL HNO_3, 2 mL HCl, and 1 mL HF. The samples were digested in a muffle furnace at 150–160 °C for 6 h and then diluted to 10 mL with ultra-pure water. The concentrations of ^{232}Th were analyzed by inductively coupled plasma mass spectrometry (ICP-MS, Thermo Elemental ×7, Waltham, USA). The background content of ^{232}Th in the filters is below the detection limit of ICP-MS (0.1 ng L^{-1}). ^{209}Bi (1.5 μg L^{-1}) was used as an internal standard to compensate for the instrument drift between runs. Quality assurance of the analytical procedure was determined by using standard solutions of both thorium and bismuth from the Beijing Research Institute of Chemical Industry and the China Institute of Metrology. Recovery was ascertained by spiking the samples with standard solutions and the average recovery varied from 89% to 96%. The coefficient of variation for replicate analysis of the samples and standards was <5%.

2.3. Data analysis

For normally distributed data, analysis of variance (ANOVA) was used to compare thorium concentration from different groups of atmospheric samples (i.e. different sampling periods and sites). For non-normally distributed data, Kruskal-Wallis test was applied instead. Meteorological data, including daily average wind speed, air pressure, temperature, vapor pressure, relative humidity and precipitation, were obtained from Baotou city meteorological stations for the period of TSP sampling. These data were used for establishing correlation patterns for thorium in TSP. To describe pattern similarity and classification of thorium pollution among the monitors, a SOM algorithm was applied to atmospheric samples and corresponding meteorological factors. The SOM is one of the most popular neural network models, which transforms multidimensional data (input data set) into one- or two-dimensional discrete map subject (output data set). The input data set consisted of seven variables including thorium concentration for 104 atmospheric samples and 6 meteorological factors. The output map is composed of an array of neurons, commonly two-dimensional hexagonal lattice. The number of map units is strongly related to the accuracy and generalization capability of SOM. An acceptable compromise between the quantization and topographic error was made to determine the number of hexagonal units by a heuristic equation, $M = 5\sqrt{N}$, where M is the number of map units, and N is the number of samples. In this study, the output map was composed of 18 neurons (6×3 hexagonal units). The output results are presented as component planes, indicating correlation patterns among the variables and natural groups based on similarity of observations. Details for implementation and properties of the SOM analysis have been described in previous studies (Lee and Scholz, 2006; Alvarez-Guerra et al., 2008). The quality of the SOM model was assessed using the quantization error (QE) and the topographic error (TE). QE is the average distance between each data point and the weight vector which is closest to the input vector (called Best-Matching Unit, BMU) and TE serves as a measurement of topology preservation, representing the proportion of all data for which the first and the second BMU are not adjacent (Kohonen, 2001). Kriging and other methods, such as the inverse distance weighted method (IDW) which have been widely applied in many scientific disciplines for spatial interpolation (Chen et al., 2009), were also conducted to confirm the results of the SOM. All interpolations were performed under the R environment (R Development Core Team, 2011).

Table 1
^{232}Th activity concentrations in TSP (mBq m^{-3}).

Sites	Periods	Mean	Std. deviation	C.V. (%)	Min	Max	Geometric mean	P-value (K-S test)
Mining areas	Mar	25.60	14.68	57.4	10.39	53.59	21.91	0.582[a]
	Aug	0.82	1.27	155.2	0.03	5.24	0.42	0.118[a]
Smelting areas	Mar	39.72	15.71	39.5	2.72	320.09	20.50	0.003
	Aug	2.81	3.44	122.4	0.04	16.65	1.41	0.011

C.V.: Coefficients of variation.
[a] Asymptotic significance > 0.05 (2-tailed).

3. Results and discussion

3.1. Activity concentrations of ^{232}Th in TSP

The descriptive statistics of ^{232}Th activity in TSP are summarized in Table 1. The Kolmogorov-Smirnov (K-S) test confirmed that the thorium concentrations in TSP in the mining area were normally distributed, whereas those in the smelting area were not normally distributed. After log-transformation, the distributions of ^{232}Th in March in the smelting area were normally distributed. The coefficient of variation (CV) can be used to compare in relative terms the variability of the same property under similar values of variances and different means. Low CV values correspond to a spatially homogeneous distribution of ^{232}Th concentrations, whereas high CV values indicate a non-homogenous surface distribution in the study area. The CVs of ^{232}Th in both mining and smelting areas in August were relatively high, >100%, indicating a high variability.

Sampling sites and periods are expected to affect concentration distribution patterns of ^{232}Th in TSP samples. Hence, we assumed that ^{232}Th concentrations in TSP are different between two sampling sites (i.e., the smelting and mining areas) and two sampling periods (i.e., 2013 March and 2012 August). ANOVA was used to determine whether the mean values of ^{232}Th concentrations collected in August 2012 differ among the defined groups, and Kruskal-Wallis test was applied for the non-normal distribution datasets. The results are listed in Table 2. Significant differences were found in ^{232}Th concentrations between two sampling periods and two sampling sites except for samples collected in March. The mean activity concentration of ^{232}Th associated with TSP in mining and smelting areas in March 2013 were 25.60 and 39.72 mBq m^{-3}, almost 31 and 14 times higher than those in August 2012. Fig. 2 shows the box-and-whisker plots of the results. ^{232}Th concentrations in TSP varied substantially over sampling time and sites, suggesting the spatial variation. Although significant difference was observed in ^{232}Th activity levels between two sampling periods, an interpretation of seasonal variation in atmospheric ^{232}Th activity levels cannot be concluded from the limited dataset in this study.

Table 2
Results of ANOVA and Kruskal-Wallis test for ^{232}Th activity concentrations in TSP samples among different defined groups.

Subgroups		Sample sites(df = 1)		Sample periods(df = 1)	
		Chi-square	Sig.	Chi-square	Sig.
^{232}Th	Smelting areas	–	–	47.19	6.44e-12[b]
	Mining areas[a]	–	–	36.88	1.74e-6[b]
	August	8.57	0.003[b]	–	–
	March	0.41	0.53	–	–

[a] ANOVA F-test.
[b] Significance level of 0.05.

It is quite clear from Table 1 and Fig. 2 that the activity concentrations of ^{232}Th in TSP were more abundant in the smelting areas than in the mining areas. This was expected and clearly indicated that the process of ore smelting must be responsible for the high atmospheric pollution load in the study area. The excessive concentration in March at the smelting and mining areas may also be attributed to the intense dust storm events originated from Taklimakan Desert, Gobi Desert and the Loess Plateau (Li et al., 2015; Zhao et al., 2015), which are known to transport large amount of radionuclides including ^{232}Th from the continental crust (Serno et al., 2014; Hirose et al., 2016).

In the literature, scientific studies and related data are limited about ^{232}Th in the atmospheric PM near the rare earth mining and smelting areas. The concentrations of ^{232}Th in TSP in the present study were more than a thousand times higher than the world reference value of 0.5 μBq m^{-3} (United Nations Scientific Committee on Effects of

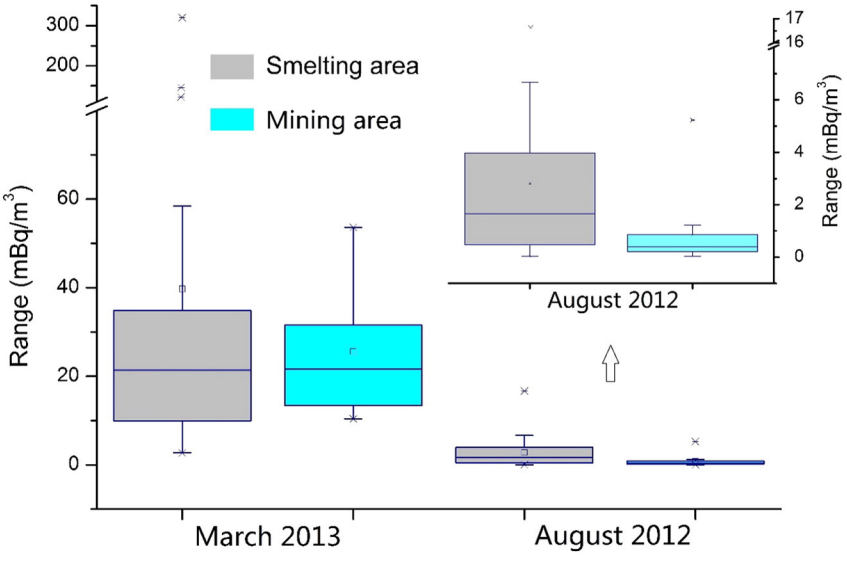

Fig. 2. ^{232}Th concentrations in the TSP.

Atomic Radiation, UNSCEAR, 2000). The concentrations of ^{232}Th observed in August were similar to previously reported levels near nuclear fuel facilities in Sweden (between 0.22 and 3.65 mBq m^{-3}, Pettersson and Holm, 1992), and the geometric mean (4.46 mBq m^{-3}) observed in both August and March approached the ambient concentration of 4.26 mBq m^{-3} reported in Canada (Ahier and Tracy, 1997).

3.2. Spatial variations of ^{232}Th in TSP

An ordinary kriging approach was applied for interpolation of atmospheric ^{232}Th in March in the smelting area, on the basis of its log-normality feature. Due to the small number of samples in the mining area and non-normality in August in the smelting area, inverse distance weighting (IDW) was used in the remaining dataset. The filled contour maps of atmospheric ^{232}Th in the mining and smelting areas are shown in Fig. 3. Compared to March, regional airflow, precipitation, and temperature resulted in low level of ^{232}Th activity in TSP in August. The spatial patterns demonstrate that hotspots of atmospheric ^{232}Th are located near a rare-earth company in the smelting area, and a water pressuring station in the mining area. The relatively high levels were observed in March at approximate 15 km in the south-west direction from a rare-earth company. No meaningful spatial gradient of ^{232}Th concentration was found in the main wind direction.

The SOM model was applied to identify the zones that were most radioactively impacted and the relationship between atmospheric ^{232}Th concentrations and meteorological factors. The component planes for correlation patterns among variables and the resulting Kohonen map are depicted in Fig. 4 and Fig. 5, respectively. The QE and TE for the 18-unit map (6×3) were 0.277 and 0, respectively, indicating a well topology-preserving mapping and its relevance to subsequent interpretation (Alvarez-Guerra et al., 2008). The U-matrix visualizes distances between neighboring map units, and helps to identify the cluster structures of the map. Each component plane shows values for each variable with its corresponding unit. Each unit represents a neuron. Sampling sites within one unit are the most similar, while sampling sites in neighboring units are more similar than sites in more distant units. The component planes which are built in color gradient allow the comparison between variables. Similar color distribution of the component planes indicates positive correlation between variables. Fig. 4 shows the relationship between ^{232}Th concentrations in TSP samples and the meteorological factors. High concentrations of atmospheric ^{232}Th are linked to higher wind speed, lower temperature, lower vapor pressure, lower

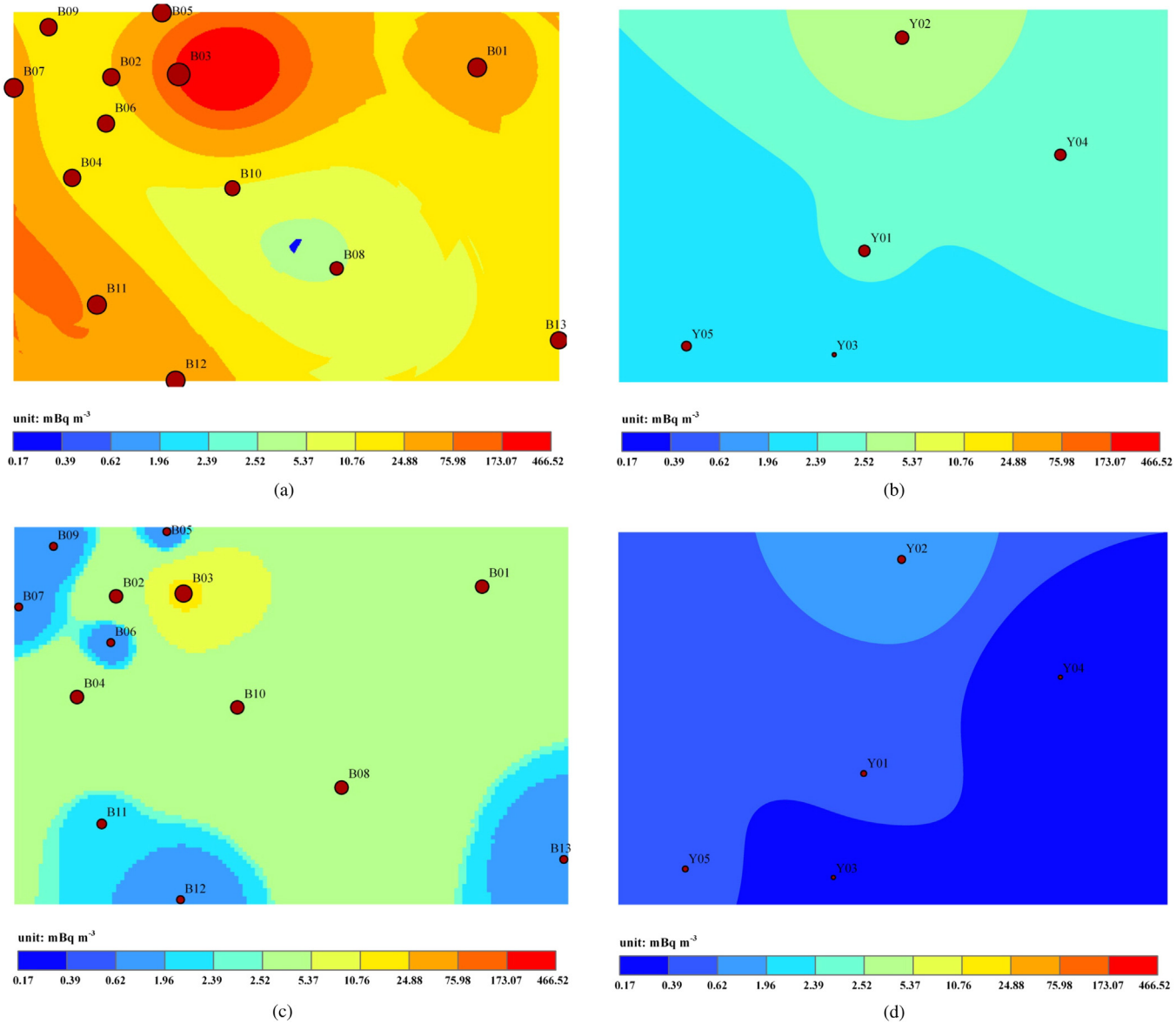

Fig. 3. Spatial distribution of ^{232}Th concentrations in TSP (a) in March in smelting area, (b) in March in mining area, (c) in August in smelting area, and (d) in August in mining area.

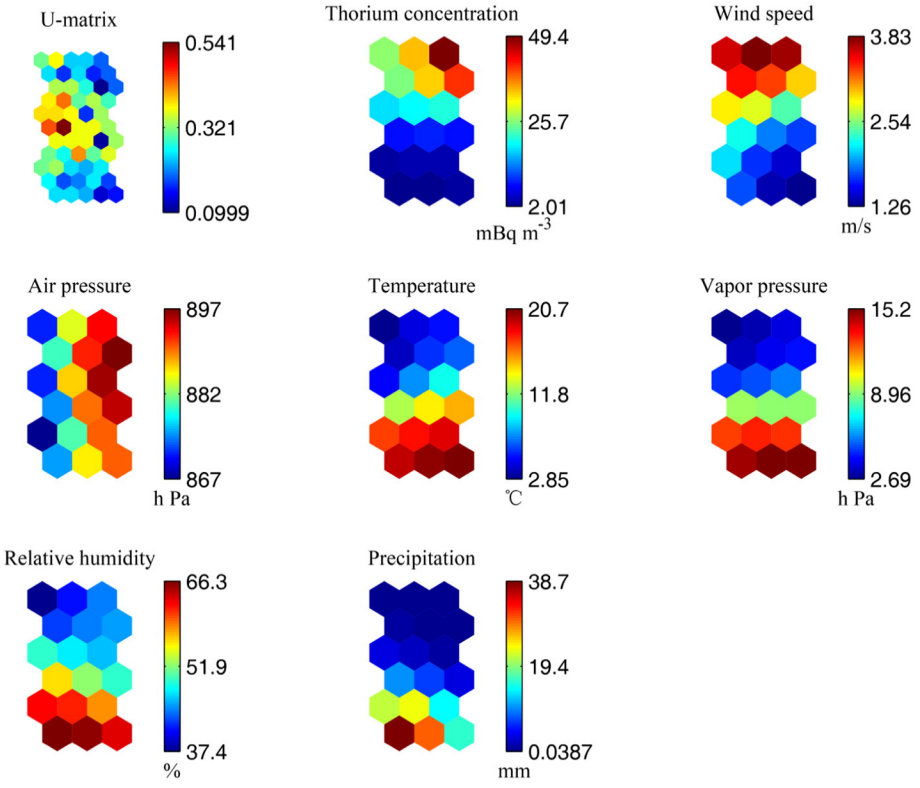

Fig. 4. Component planes of the Self-organizing Maps for 7 input variables. Visualization of the relationship between thorium concentrations in TSP and meteorological factors.

relative humidity, and lower precipitation in March than in August. A decrease in daily average temperature, vapor pressure, relative humidity, and precipitation from August to the next March corresponds with an increase of the atmospheric ^{232}Th concentrations, suggesting that meteorology is one of the main mechanistic determinant factors. Moreover, the elevated ^{232}Th level in March is probably due to thorium-enriched aerosol transported from the continental crust by the intensive dust storm. The Kohonen resulting map for atmospheric ^{232}Th were grouped into four classes according to the sampling time (i.e. March and August) and zones (smelting area and mining area). For spatial variation, most samples showed relatively low concentrations of ^{232}Th, while three hotspots were identified in the smelting area with high radioactive pollution. Only sample B03 surrounding two rare earth smelters is a real point source of thorium pollution, whereas the other two samples B11 and B12 which were at approximately 15 km southwest from the rare earth smelters are probably related to transport of ^{232}Th.

3.3. Inhalation exposure

^{232}Th concentrations measured in PM_{10} samples collected in the vicinity of the rare earth mining and smelting areas were used for health risk assessment. The inhalation annual effective radiation dose (E_h) associated with PM_{10} was calculated using the following equation adapted from United Nations Scientific Committee on Effects of Atomic Radiation (UNSCEAR) (2000):

$$E_h = C_a \times B \times d_h \times (1 - F_o + F_o F_r)$$

where C_a is the integrated activity concentration of ^{232}Th associated with PM_{10} (Bq m^{-3}), B is the breathing rate (m^3 year^{-1}), d_h is the committed dose per unit intake from inhalation or effective dose coefficient (Sv Bq^{-1}), F_o is the indoor occupancy factor and F_r is the ratio of indoor to outdoor air concentration.

The annual effective radiation dose due to inhalation of PM_{10} was calculated for the six age groups identified by International Commission of Radiological Protection (The International Commission on Radiological Protection, ICRP, 2012), namely 3 month, 1, 5, 10, and 15 years, and adults. For each age group, the corresponding coefficients recommended by ICRP were used. The ratio of indoor to outdoor air concentration (F_r) was assumed to be 0.3 (United Nations Scientific Committee on Effects of Atomic Radiation, UNSCEAR, 2000). The values used for the different age groups are summarized in Table 3.

The mean activity concentrations of ^{232}Th at the sampling sites of mining and smelting areas were 5.97 mBq m^{-3} (1.81–11.62 mBq m^{-3}) and 5.79 mBq m^{-3} (2.38–11.82 mBq m^{-3}), respectively. The average activity concentrations were used to calculate the inhalation annual effective radiation dose for various age groups at different sampling sites. Because of the variations in air breathing rate, the total annual dose due to the natural radioactivity in airborne PM_{10} increases for the older age groups. The mean values of dose for the different age groups in smelting and mining areas ranged from 97.86 to 417 μSv year^{-1} and from 101.03 to 430.83 μSv year^{-1}, respectively. These annual effective doses are lower than the annual limit of 1 mSv year^{-1} as suggested by the ICRP. But it does not mean that people living in the study areas are safe. These dose values only present the inhalation exposure associated with the PM_{10} fraction of atmospheric particles. The total annual effective doses received by the general public also include the external gamma radiation, inhalation and ingestion exposures to all radioactive nuclides (Iwaoka et al., 2013). The results of the present study are significantly higher than the inhalation radiation dose reported in Jeddah City, Saudi Arabia (15.03–58.87 nSv year^{-1}). This indicates potential high risk of ^{232}Th exposure in both the rare earth mining and smelting regions.

4. Conclusions

The results of this study showed that ^{232}Th concentrations in TSP varied substantially over sampling sites, suggesting great spatial

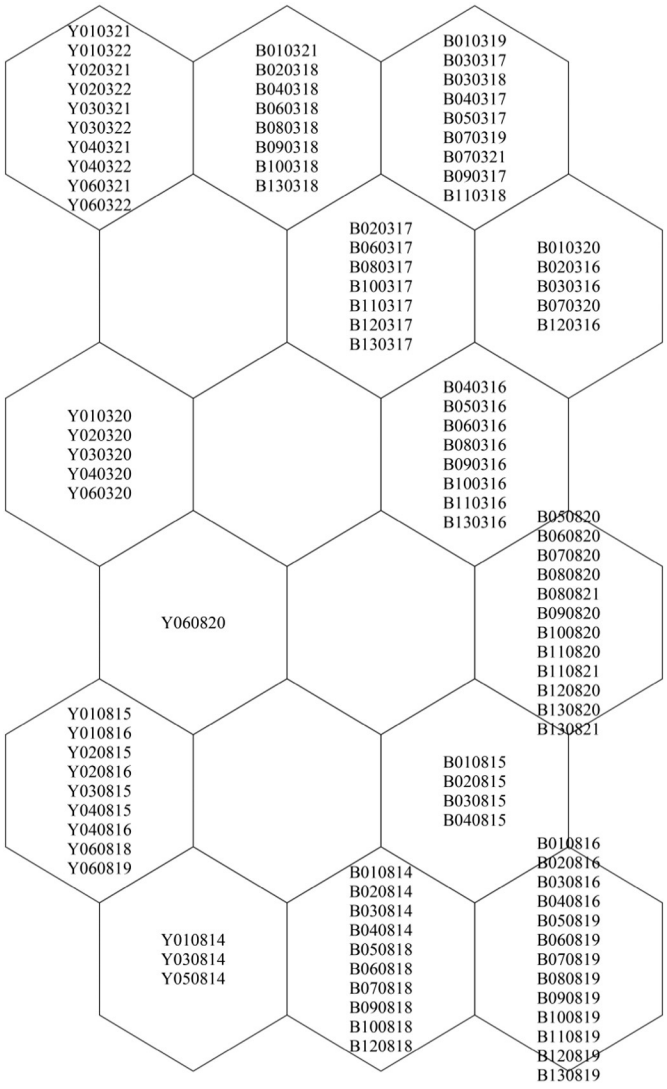

Fig. 5. Kohonen self-organizing map for ^{232}Th in TSP samples. Sampling sites within one cell share similar pattern. For each label, i.e. B030317, the first three characters "B03" represent sampling NO., the last four characters "0317" represent sampling date.

variations. Although significant difference were observed in ^{232}Th activity levels collected in August and March, to what extent the seasonal variation exists in atmospheric 232Th activity levels requires a long-term study in the future. The relatively high concentration in March at the smelting and mining areas can be attributed to frequent dust storms in spring in this region. Under the meteorological conditions during the sampling period in this study, results showed that regional airflow, precipitation, relative humidity, and temperature were the main factors affecting atmospheric ^{232}Th removal. However, more studies are needed for long-term data collection to conclude on the relationship between atmospheric ^{232}Th activity levels and meteorological factor. Atmospheric thorium samples were grouped into four classes according to the sampling time and zones. One real hotspot was observed at a sampling location near a rare-earth company. The results of the inhalation exposure emphasize the importance and significance of the potential radiation risk. This study demonstrated that a combination of multivariate statistics and SOM map can serve as a useful tool to characterize ^{232}Th spatial distribution and to determine the pollution sources. The results of this study call for effective polices on protecting human health from long-term inhalation exposure to radioactive pollution in the study area.

Table 3
The average inhalation annual effective radiation dose for various age groups.

Age group	3 mo.	1 year	5 year	10 year	15 year	Adult
Breathing rate, B (m^3 d^{-1})	2.86	5.16	8.72	15.3	20.1	22.2
Indoor occupancy factor, F_o	1.0	0.96	0.88	0.88	0.9	0.92
Effective dose coefficient, d_h(μSv Bq^{-1})	54.00	50.00	37.00	26.00	25.00	25.00
Inhalation annual effective radiation dose (μSv $year^{-1}$)						
Smelting areas	97.86	178.75	261.70	322.66	392.72	417.34
Mining areas	101.03	184.52	270.15	333.08	405.41	430.83

Acknowledgments

This study was sponsored by the National Natural Science Foundation of China (No. 41401591 and 41571473).

References

Aguado, D., Montoya, T., Borras, L., Seco, A., Ferrer, J., 2008. Using SOM and PCA for analysing and interpreting data from a P-removal SBR. Eng. Appl. Artif. Intell. 21 (6), 919–930.
Ahier, B.A., Tracy, B.L., 1997. Evaluating the radiological impact of uranium emissions in port hope, Ontario—a comparison of monitoring and modelling results. J. Environ. Radioact. 34 (2), 187–205.
Alvarado, J.C., Steinmann, P., Estier, S., Bochud, F., Haldimann, M., Froidevaux, P., 2014. Anthropogenic radionuclides in atmospheric air over Switzerland during the last few decades. Nat. Commun. 5, 3030.
Alvarez-Guerra, M., González-Piñuela, C., Andrés, A., Galán, B., Viguri, J.R., 2008. Assessment of self-organizing map artificial neural networks for the classification of sediment quality. Environ. Int. 34 (6), 782–790.
Ault, T., Krahn, S., Croff, A., 2015. Radiological impacts and regulation of rare earth elements in non-nuclear energy production. Energy 8 (3), 2066–2081.
Binnemans, K., Jones, P.T., 2015. Rare earths and the balance problem. J. Sustain. Metall. 1 (1), 29–38.
Chen, X.A., Cheng, Y.E., Rong, Z., 2005. Recent results from a study of thorium lung burdens and health effects among miners in China. J. Radiol. Prot. 25 (4), 451.
Chen, X.A., Cheng, Y.E., Xiao, H., Feng, G., Deng, Y.H., Feng, Z.L., Zheng, R., 2004. Health effects following long-term exposure to thorium dusts: a twenty-year follow-up study in China. Radioprotection 39 (04), 525–533.
Chen, T., Liu, X., Li, X., Zhao, K., Zhang, J., Xu, J., Shi, J., Dahlgren, R.A., 2009. Heavy metal sources identification and sampling uncertainty analysis in a field-scale vegetable soil of Hangzhou, China. Environ. Pollut. 157 (3), 1003–1010.
Cowart, J.B., Burnett, W.C., 1994. The distribution of uranium and thorium decay-series radionuclides in the environment-a review. J. Environ. Qual. 23 (4), 651–662.
Garćia, H.L., González, I.M., 2004. Self-organizing map and clustering for wastewater treatment monitoring. Eng. Appl. Artif. Intell. 17 (3), 215–225.
Gulson, B., Korsch, M., Dickson, B., Cohen, D., Mizon, K., Davis, J.M., 2007. Comparison of lead isotopes with source apportionment models, including SOM, for air particulates. Sci. Total Environ. 381 (1), 169–179.
Hao, Z., Li, Y., Li, H., Wei, B., Liao, X., Liang, T., Yu, J., 2015. Levels of rare earth elements, heavy metals and uranium in a population living in Baiyun Obo, Inner Mongolia, China: A pilot study. Chemosphere 128, 161–170.
Hirose, K., Kikawada, Y., Igarashi, Y., Fujiwara, H., Jugder, D., Matsumoto, Y., Nomura, M.A.S.A.O., 2016. Plutonium, 137 Cs and uranium isotopes in Mongolian surface soils. J. Environ. Radioact. http://dx.doi.org/10.1016/j.jenvrad.2016.01.007 (in press).
Höllriegl, V., Greiter, M., Giussani, A., Gerstmann, U., Michalke, B., Roth, P., Oeh, U., 2007. Observation of changes in urinary excretion of thorium in humans following ingestion of a therapeutic soil. J. Environ. Radioact. 95 (2), 149–160.
Hong, Y.S.T., Rosen, M.R., Bhamidimarri, R., 2003. Analysis of a municipal wastewater treatment plant using a neural network-based pattern analysis. Water Res. 37 (7), 1608–1618.
Iwaoka, K., Tabe, H., Yonehara, H., 2013. Natural radioactivity of bedrock bath instruments and hot spring instruments in Japan. J. Radioanal. Nucl. Chem. 295 (2), 817–821.
Kohonen, T., 2001. Self-Organizing Maps. third ed. Springer, Berlin, Germany.
Kritsananuwat, R., Sahoo, S.K., Fukushi, M., Chanyotha, S., 2015. Distribution of rare earth elements, thorium and uranium in Gulf of Thailand's sediments. Environ. Earth Sci. 73 (7), 3361–3374.
Lee, B.H., Scholz, M., 2006. Application of the self-organizing map (SOM) to assess the heavy metal removal performance in experimental constructed wetlands. Water Res. 40 (18), 3367–3374.
Li, R., Gong, J., Zhou, J., Sun, W., Ibrahim, A.N., 2015. Multi-satellite observation of an intense dust event over southwestern China. Aerosol Air Qual. Res. 15 (1), 263–270.
Li, S.G., Harazono, Y., Zhao, H.L., He, Z.Y., Chang, X.L., Zhao, X.Y., Oikawa, T., 2002. Micrometeorological changes following establishment of artificially established artemisia vegetation on desertified sandy land in the Horqin sandy land, China and their implication on regional environmental change. J. Arid Environ. 52 (1), 101–119.

Li, R.Y., Li, Q., Chen, S., Wu, F.C., Sun, D.Z., Liao, H.Q., 2014. Distribution of thorium in soils surrounding the rare-earth tailings reservoir in Baotou, China. J. Radioanal. Nucl. Chem. 299 (3), 1453–1459.

Mari, M., Nadal, M., Schuhmacher, M., Domingo, J.L., 2010. Application of self-organizing maps for PCDD/F pattern recognition of environmental and biological samples to evaluate the impact of a hazardous waste incinerator. Environ. Sci. Technol. 44 (8), 3162–3168.

Mukherjee, A., 1997. Self-organizing neural network for identification of natural modes. J. Comput. Civ. Eng. 11 (1), 74–77.

Nadal, M., Kumar, V., Schuhmacher, M., Domingo, J.L., 2006. Definition and GIS-based characterization of an integral risk index applied to a chemical/petrochemical area. Chemosphere 64 (9), 1526–1535.

Pettersson, H.B.L., Holm, E., 1992. Investigation of aerial dispersion of uranium isotopes from a nuclear fuel fabrication facility. Waste Manag. 12 (1), 85–97.

R Development Core Team, 2011. R: A Language and Environment for Statistical Computing. R Foundation for Statistical Computing, Vienna, Austria (Open access available at) http://cran.r-project.org.

Serno, S., Winckler, G., Anderson, R.F., Hayes, C.T., McGee, D., Machalett, B., Haug, G.H., 2014. Eolian dust input to the Subarctic North Pacific. Earth Planet. Sci. Lett. 387, 252–263.

Soudek, P., Kufner, D., Petrová, Š., Mihaljevič, M., Vaněk, T., 2013. Composition of hydroponic medium affects thorium uptake by tobacco plants. Chemosphere 92 (9), 1090–1098.

The International Commission on Radiological Protection (ICRP), 2012C. Compendium of dose coefficients based on ICRP publication 60 ICRP publication 119 Ann. ICRP 41 (Suppl.).

United Nations Scientific Committee on Effects of Atomic Radiation (UNSCEAR), 2000a. Report to the General Assembly. Sources and Effects of Ionizing Radiation. Vol. I (New York).

Wu, C., 2008. Bayan Obo controversy: carbonatites versus iron oxide-Cu-Au-(REE-U). Resour. Geol. 58 (4), 348–354.

Zhao, S., Yu, Y., Xia, D., Yin, D., He, J., Liu, N., Li, F., 2015. Urban particle size distributions during two contrasting dust events originating from Taklimakan and Gobi Deserts. Environ. Pollut. 207, 107–122.

Zhu, Z., Pranolo, Y., Cheng, C.Y., 2015. Separation of uranium and thorium from rare earths for rare earth production-a review. Miner. Eng. 77, 185–196.